ELSEVIER

Composites: Part B 32 (2001) 491–502

composites
Part B: engineering

www.elsevier.com/locate/compositesb

Mechanics of bonds in an FRP bonded concrete beam

K.T. Lau[a,*], P.K. Dutta[b], L.M. Zhou[a], D. Hui[c]

[a]Department of Mechanical Engineering, The Hong Kong Polytechnic University, Hong Kong, People's Republic of China
[b]Cold Region Research and Engineering Laboratory, Hanover, NH 03755, USA
[c]Department of Mechanical Engineering, University of New Orleans, USA

Received 22 February 2001; accepted 29 May 2001

Abstract

Fibre-reinforced plastic (FRP) materials have been recognised as new innovative materials for concrete rehabilitation and retrofit. Since concrete is poor in tension, a beam without any form of reinforcement will fail when subjected to a relatively small tensile load. Therefore, the use of the FRP to strengthen the concrete is an effective solution to increase the overall strength of the structure. The attractive benefits of using FRP in real-life civil concrete applications include its high strength to weight ratio, its resistance to corrosion, and its ease of moulding into complex shapes without increasing manufacturing costs. The speed of application minimises the time of closure of a structure compared to other strengthening methods. In this paper, a simple theoretical model to estimate shear and peel-off stresses is proposed. Axial stresses in an FRP-strengthened concrete beam are considered, including the variation in FRP plate fibre orientation. The theoretical predictions are compared with solutions from an experimentally validated finite element model. The results from the theory show that maximum shear and peel-off stresses are located in the end region of the FRP plate. The magnitude of the maximum shear stress increases with increases in the amount of fibres aligned in the beam's longitudinal axis, the modulus of an adhesive material and the number of laminate layers. However, the maximum peel-off stress decreases with increasing thickness of the adhesive layer.

Keywords: A. Fibres; Concrete strengthening

1. Introduction

Over the past several decades, extensive research and development in the field of materials engineering and science have been carried out with fibre-reinforced plastic (FRP) composites leading to a wide range of practical applications [1,2]. Conventional rehabilitating techniques using stitching and steel reinforcing patch design provide a promising strengthening solution in civil concrete applications [3]. Unfortunately, the weight penalty, labour intensive application, and subsequent corrosion of the steel material may eventually increase the overall maintenance cost [4]. Accordingly, this drives the development and application of new materials and technologies, which extend the service life of many structures, such as strengthening of structures to carry greater traffic loads, to cope with change of use, to rectify design faults, and for repair. Thus, the use of FRP materials is becoming increasingly important for extending the service life of our civil construction facilities into the 21st century [5].

Steel plate bonding is recognised as an effective solution for reinforcing or strengthening concrete elements in order to minimise the risk of concrete cracking, which may result in the corrosion of embedded steel reinforcement. Eventually, surface concrete may spall due to the volumetric expansion of the corroded steel material.

The use of FRP in upgrading and strengthening civil concrete structures has been accepted gradually only in recent years. In the past, FRP materials were used primarily in the aerospace and defence industries rather than in civil construction areas, mainly due to the prohibitively high cost of raw materials and manufacturing processes. Previous researches showed that glass fibre composites could be effectively used for concrete beam strengthening, resulting in the improvement of flexural load carrying capacity [6–10]. Among all different types of concrete strengthening methods, the use of FRP materials for tension face strengthening techniques presents better strengthening characteristic in terms of the ultimate flexural load capacity [11,12]. This paper introduces a theoretical model for estimating adhesive shear and peel-off stresses, and the normal stress of an

* Corresponding author. Tel.: +86-852-2766-7730; fax: +86-852-2365-4703.
E-mail address: mmktlau@polyu.edu.hk (K.T. Lau).

1359-8368/01/$ - see front matter
PII: S1359-8368(01)00032-4

externally bonded FRP plate on the beam tension surface with different fibre orientations, laminate layers, and mechanical properties of the FRP and adhesive materials for the FRP-strengthened concrete structure.

2. Theoretical approach

A concrete model, which is designed for a concrete beam strengthened by an FRP plate on its tension surface subjecting to a three-point bending test, is used for present study. A schematic illustration of a theoretical model for evaluating the adhesive stress transfer properties for the current study is shown in Fig. 1. The following assumptions are used to simplify the calculations:

1. The concrete, adhesive, and FRP materials behave elastically, linearly, and isotropically.
2. No slip is allowed at the interface of the bond (i.e. there is a perfect bond between the FRP plate and the concrete).
3. Stresses in the adhesive layer and FRP plate do not change with thickness because it is assumed that both the adhesive and composite materials are very thin.
4. The bending stiffness of the concrete beam to be strengthened is much greater than the stiffness of the composite plate.

2.1. Adhesive shear stress

Adhesive shear failure is one of the most common failure patterns that may happen in plate-bonded concrete structures as shown in Fig. 2. An excess of applied shear stress in the adhesive layer leads to failure at the interface between the concrete beam and the FRP plate and results in the reduction of the effective bonding length of the plate. In Fig. 1, the compatibility expression for the shear stress τ_a in the adhesive layer at any section x is given by

$$\tau_a(x) = \frac{G_a}{t_a}[u_p(x) - u_c(x)], \tag{1}$$

where G_a, t_a, u_c and u_p denote the shear modulus, the thickness of the adhesive material, the displacement of the concrete, and the displacement of the externally bonded FRP plate at the boundary of the bond, respectively. Eq. (1) can be expressed in terms of the mechanical strain of the concrete, $\epsilon_c(x)$, and the FRP plate $\epsilon_p(x)$ after differentiating the equation with respect to x

$$\frac{d\tau_a(x)}{dx} = \frac{G_a}{t_a}[\epsilon_p(x) - \epsilon_c(x)], \tag{2}$$

where

$$\frac{du_c(x)}{dx} = \epsilon_c(x) \tag{3a}$$

and

$$\frac{du_p(x)}{dx} = \epsilon_p(x). \tag{3b}$$

The tensile strain at the bottom of the beam is induced by two basic stress components: (1) the tensile stress induced by the bending moment $M_c(x)$ in the beam and (2) the axial stress induced by the adhesive shear stress at the bond interface. Therefore, Eqs. (3a) and (3b) can be written as

$$\epsilon_c(x) = \frac{1}{E_c\omega h^2}[6M_c(x) - N_c(x)h] \tag{4}$$

and

$$\epsilon_p(x) = \frac{N_p(x)}{\omega t_p E_{eff}}, \tag{5}$$

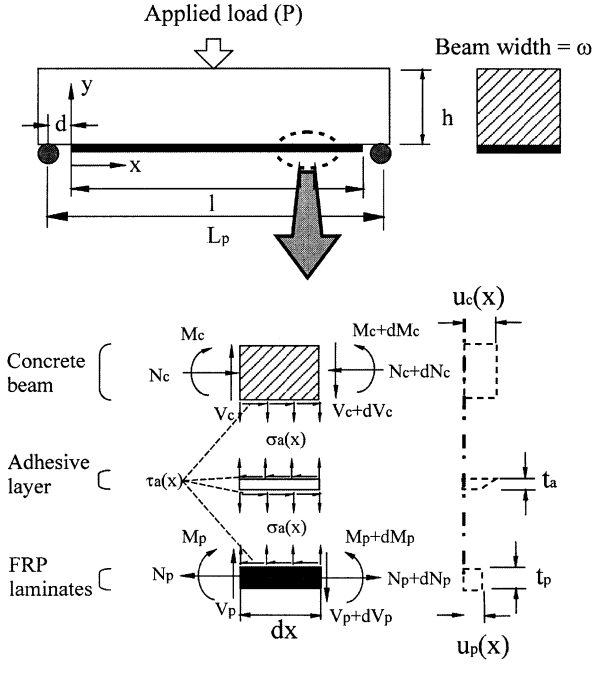

Stresses mechanics for the concrete strengthened by FRP laminates

Fig. 1. Theoretical model for the present study.

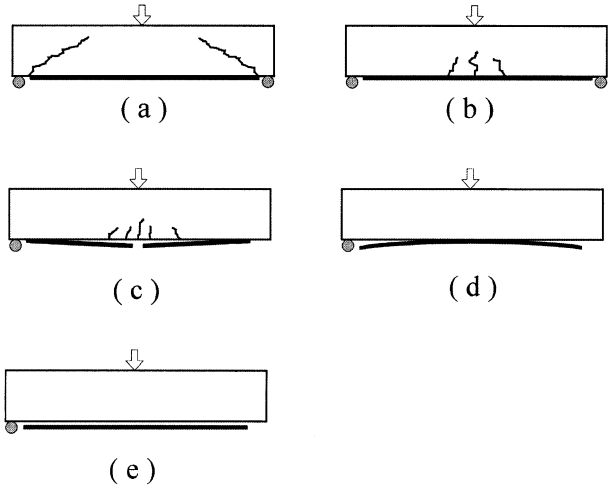

Fig. 2. Typical failure patterns of plate-bonded concrete structures.

where t_p and E_{eff} represent the thickness and effective modulus of the composite plate, respectively. E_c, ω, h, and N_c represent the modulus of the concrete, the width and height of the beam, and the axial load of the beam, respectively. Since the composite laminate is an orthotropic material, its material properties vary from layer to layer. In current study, the laminate theory is used to determine the stress and strain behaviours of the externally bonded composite plate in order to investigate the whole mechanical performance of the composite-strengthened structure. The effective modulus of the composite laminate is varied by the orientation of the fibre directions and arrangements of the laminate patterns. Eq. (5) is only valid for the plate for which the mechanical properties behave isotropically and homogeneously. Therefore, the laminate theory is used to estimate the strain of the composite plate [13], i.e.

$$\begin{Bmatrix} \boldsymbol{\epsilon}^0 \\ \mathbf{M} \end{Bmatrix} = \begin{bmatrix} \mathbf{A}^x & \mathbf{B}^x \\ \mathbf{C}^x & \mathbf{D}^x \end{bmatrix} \begin{Bmatrix} N \\ k \end{Bmatrix}, \tag{6a}$$

where $[\mathbf{A}^x] : [\mathbf{A}^{-1}]$, $[\mathbf{B}^x] : [\mathbf{A}^{-1}][\mathbf{B}]$, $[\mathbf{C}^x] : [\mathbf{B}][\mathbf{A}^{-1}]$, $[\mathbf{D}^x] : [\mathbf{D}] - [\mathbf{B}][\mathbf{A}^{-1}][\mathbf{B}]$ and

$$\text{Extensional matrix} \qquad \mathbf{A}_{ij} = \sum_{k=1}^{n} (\bar{Q}_{ij})_k (z_k - z_{k-1}), \tag{6b}$$

Extensional-bending coupled ***matrix***

$$\mathbf{B}_{ij} = \frac{1}{2} \sum_{k=1}^{n} (\bar{Q}_{ij})_k (z_k^2 - z_{k-1}^2), \tag{6c}$$

$$\text{Flexural matrix} \qquad \mathbf{D}_{ij} = \frac{1}{3} \sum_{k=1}^{n} (\bar{Q}_{ij})_k (z_k^3 - z_{k-1}^3). \tag{6d}$$

The subscript n represents the number of laminate layers of the FRP plate. Parameter $\bar{Q}_{ij}$ can be estimated by using the off-axis orthotropic ply theory [13]. A schematic diagram illustrating the laminate theory for a composite plate is shown in Fig. 3. Assume that the ply arrangement of the plate is symmetrical with respect to the mid-plane axis $z = 0$. A great simplification in laminate analysis then occurs by assuming that the coupling matrix **B** is identically zero [14]. Furthermore, it is assumed that no external bending moment is applied to the plate. Therefore Eqs. (6a)–(6d) can be simplified to the following matrix form for a plate with a width of ω:

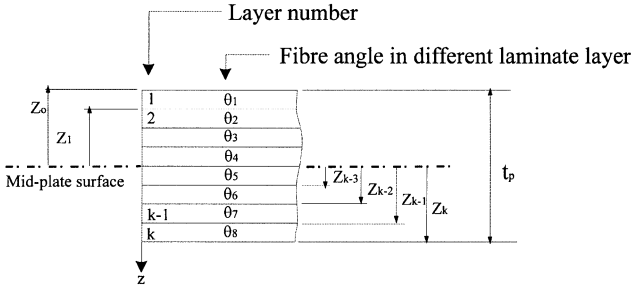

Fig. 3. Multi-layered laminate geometry.

$$\{\boldsymbol{\epsilon}^0\} = [\mathbf{A}^x]\{N\}_p, \tag{7}$$

where

$$\{\boldsymbol{\epsilon}^0\} = \begin{Bmatrix} \epsilon_x \\ \epsilon_y \\ \epsilon_{xy} \end{Bmatrix} \quad \text{and} \quad \{N\}_p = \begin{Bmatrix} N_x \\ N_y \\ N_{xy} \end{Bmatrix}_p. \tag{8}$$

In the present study, only an axial load in the beam's longitudinal axis is considered, i.e. $N_y = N_{xy} = 0$. Therefore, Eq. (7) can be simplified to

$$\epsilon_p(x) = \mathbf{A}_{11}^x N_x \frac{1}{\omega}. \tag{9}$$

If we differentiate Eq. (2) by considering the strains given by Eqs. (4) and (9), we obtain

$$\frac{\mathrm{d}\tau_a^2(x)}{\mathrm{d}x^2} = \frac{G_a}{t_a}\left[\frac{\mathbf{A}_{11}^x}{\omega}\frac{\mathrm{d}N_p(x)}{\mathrm{d}x} - \left(\frac{6}{\omega h^2}\frac{\mathrm{d}M_c(x)}{\mathrm{d}x} - \frac{1}{\omega h^2}\frac{\mathrm{d}N_c(x)}{\mathrm{d}x}\right)\right]. \tag{10}$$

The bending moment in the beam $M_c(x)$ is determined by the sum of an external applied moment due to the centre load P and a moment induced by the adhesive shear force:

$$\mathrm{d}M_c(x) = R_b\,\mathrm{d}x - \tau_a(x)\omega\,\mathrm{d}x\frac{h}{2}, \tag{11}$$

where R_b is the reaction force at the support. For a three-point bending case, $R_b = P/2$. The axial load applied in the concrete is

$$\mathrm{d}N_c(x) = \tau_a(x)\omega\,\mathrm{d}x. \tag{12a}$$

The magnitude of the axial tension load in the FRP plate is determined by the amount of adhesive shear force transferred from the concrete beam to the FRP plate, i.e.

$$\mathrm{d}N_p(x) = \tau_a(x)\omega\,\mathrm{d}x. \tag{12b}$$

Substituting Eqs. (11)–(12b) in Eq. (10) gives the following equation:

$$\frac{\mathrm{d}^2\tau_a(x)}{\mathrm{d}x^2} = \frac{G_a\omega}{t_a}\left(\frac{\mathbf{A}_{11}^x}{\omega} + \frac{4}{\omega h E_c}\right)\tau_a(x) - \frac{6R_bG_a}{E_c\omega h^2 t_a}. \tag{13}$$

The mathematical solution for Eq. (13) is

$$\tau_a(x) = C_1\cosh(\beta x) + C_2\sinh(\beta x) + \eta_0, \tag{14}$$

where

$$\beta = \sqrt{\frac{G_a\omega}{t_a}\left(\frac{\mathbf{A}_{11}^x}{\omega} + \frac{4}{\omega h E_c}\right)} \tag{15a}$$

and

$$\eta_0 = \frac{6R_b G_a}{E_c \omega h^2 t_a \beta^2}. \tag{15b}$$

where C_1 and C_2 are arbitrary constants that are determined by using appropriate boundary conditions. The first and second derivatives of Eq. (14) with respect to x are given by

$$\frac{d\tau_a(x)}{dx} = C_1\beta \sinh(\beta x) + C_2\beta \cosh(\beta x) \tag{16}$$

and

$$\frac{d^2\tau_a(x)}{dx^2} = C_1\beta^2 \cosh(\beta x) + C_2\beta^2 \sinh(\beta x). \tag{17}$$

For the three-point bending test model, it is shown that there is no axial component force, which is induced by the adhesive shear stress as indicated in Eqs. (12a) and (12b) in the beam's longitudinal direction at $z = 0$ in the concrete and FRP plate, i.e. $N_P(0) = N_c(0) = 0$. However, the bending moment M_c at the plate end region is equal to the vertical reaction force, R_b at the support multiplied by the distance from the support to the plate end d. By considering the first boundary condition, the first derivative of Eq. (2) yields:

$$\frac{d\tau_a(x)}{dx} = \frac{G_a}{t_a}\left[\frac{\mathbf{A}_{11}^x}{\omega}N_p(0) - \frac{1}{E_c}\left(\frac{6}{\omega h^2}M_c(0) - \frac{1}{\omega h}N_c(0)\right)\right], \tag{18a}$$

$$\frac{d\tau_a(x)}{dx} = C_1\beta \sinh(\beta\cdot 0) + C_2\beta \cosh(\beta\cdot 0). \tag{18b}$$

The coefficient of C_2 is

$$C_2 = \frac{6G_a R_b d}{E_c t_a \omega h^2 \beta}. \tag{19}$$

As the model is symmetrical about the middle axis of the beam, the adhesive shear stress $\tau_a(x)$ is theoretically equal to zero when $x = l/2$. So, the second boundary condition is given by:

$$\tau_a\left(\frac{1}{2}\right) = 0. \tag{20}$$

Eq. (14) becomes

$$C_1 \cosh\left(\beta\frac{1}{2}\right) + C_2 \sinh\left(\beta\frac{1}{2}\right) + \eta_0 = 0 \tag{21}$$

and therefore

$$C_1 + C_2 \tanh\left(\beta\frac{1}{2}\right) - \frac{\eta_0}{\cosh\left(\beta\frac{1}{2}\right)} = 0. \tag{22}$$

Since the third terms in Eq. (22) can be neglected (≈ 0) for $\beta 1 > 10$ [17], the coefficient C_1 yields

$$C_1 = \frac{6G_a R_b d}{E_c t_a \omega h^2 \beta}\tanh\left(\frac{\beta l}{2}\right). \tag{23}$$

The parabolic function in Eq. (23) can be assumed to be equal to 1 when the value inside the bracket is greater than 4. Hence, the full equation of the adhesive shear stress distribution along the bond line measured from the plate end ($x = 0$) can be written as

$$\tau_a(x) = C_1[\cosh(\beta x) - \sinh(\beta x)] + \eta_0. \tag{24}$$

The parabolic functions of $\cosh(\beta x)$ and $\sinh(\beta x)$ can be expressed in exponential forms:

$$\cosh(\beta x) = \frac{e^{\beta x} + e^{-\beta x}}{2} \tag{25a}$$

and

$$\sinh(\beta x) = \frac{e^{\beta x} - e^{-\beta x}}{2}. \tag{25b}$$

Therefore, Eq. (24) can be simplified to

$$\tau_a(x) = C_1\, e^{-\beta x} + \eta_0. \tag{26}$$

The axial force in the FRP plate in the beam direction $N_p(x)$ can be determined by integrating Eq. (12b) with the substitution of Eq. (26). The same boundary condition is used at the plate end region, i.e. $N_p(0) = 0$:

$$N_p(x) = C_1\left(\frac{\omega}{\beta}(1 - e^{-\beta x}) + \frac{\omega}{d\beta}x\right). \tag{27}$$

In general, the maximum adhesive shear stress is located at the short end ($x = 0$) of the externally bonded FRP plate, while the maximum tensile load added on the plate is located at the mid-beam ($x = l/2$) region. It is then possible to write Eqs. (26) and (27) when they achieve in the ultimate stress and load conditions as

$$\tau_{a,max} = C_1 + \eta_0 \tag{28a}$$

and

$$N_{p,max} = \frac{C_1\omega}{\beta}\left(1 + \frac{l}{2d}\right). \tag{28b}$$

Eqs. (28a) and (28b) show that the maximum adhesive shear stress is only dependent on the coefficient of C_1. It means that the shear stress increases with increasing shear modulus and decreasing thickness of the adhesive material.

2.2. Adhesive peel-off stress

Peel-off is another common mode of failure for the FRP-plate-strengthened concrete structure when it is subjected to bending. Fig. 4 shows a peel-off failure at the interface of bond of the glass fibre composite strengthened concrete beam [15]; no visible damage in concrete was found. Triantafillou et al. [16] found experimentally that peel-off failure of concrete strengthened by a carbon fibre composite on its tension surface occurred followed by diagonal cracking in the concrete. The results from his experiment were used to validate the model, as described in later in this paper. Therefore, in-depth investigation of the mechanical performance,

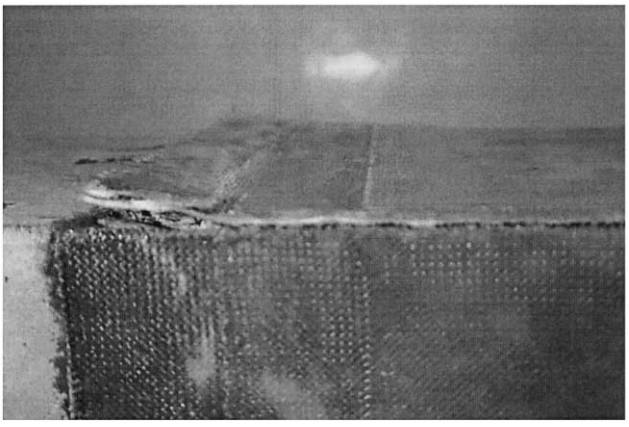

Fig. 4. Peel-off failure of a glass fibre composite strengthened concrete beam.

particularly for the adhesive peel-off stress of the plate-bonded structure, is essential.

The peel-off stress in the adhesive layer at any section of x can be simply defined as:

$$\sigma_{\mathrm{a}}^{z}(x) = E_{\mathrm{a}} \frac{v_{\mathrm{p}}^{z}(x) - v_{\mathrm{c}}^{z}(x)}{t_{\mathrm{a}}}, \tag{29}$$

where σ_{a}^{z}, t_{a}, E_{a} and v represent the peel-off stress, the thickness and tensile modulus of the adhesive material, and the deformation of material in z direction, respectively. Subscripts p, c and a denote the externally bonded FRP plate, concrete and adhesive materials, respectively. The superscript z represents the direction of deformation. The bending moment M_{p} in a small element of the externally bonded FRP plate with a length and thickness of dx and t_{a} as showed in Fig. 5 is given by:

$$\mathrm{d}M_{\mathrm{p}}(x) = V_{\mathrm{p}}^{z}(x)\,\mathrm{d}x - \tau_{\mathrm{a}}(x)\omega\frac{t_{\mathrm{p}}}{2}\mathrm{d}x, \tag{30}$$

where $V_{\mathrm{p}}^{z}(x)$ is a shear force, which is measured from the shear force diagram as indicted in Fig. 6, of the externally bonded FRP plate at any section of x. Differentiating Eq. (30), we obtain

$$\frac{\mathrm{d}^2 M_{\mathrm{p}}(x)}{\mathrm{d}x^2} = \frac{\mathrm{d}V_{\mathrm{p}}^{z}(x)}{\mathrm{d}x} - \frac{\mathrm{d}\tau_{\mathrm{a}}(x)}{\mathrm{d}x}\frac{t_{\mathrm{p}}}{2}\omega. \tag{31}$$

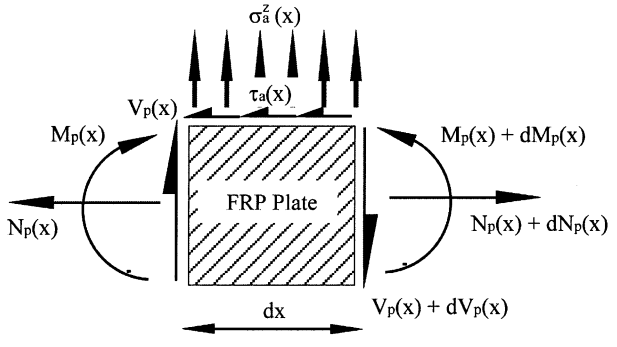

Fig. 5. Small element of the FRP plate with a length of dx.

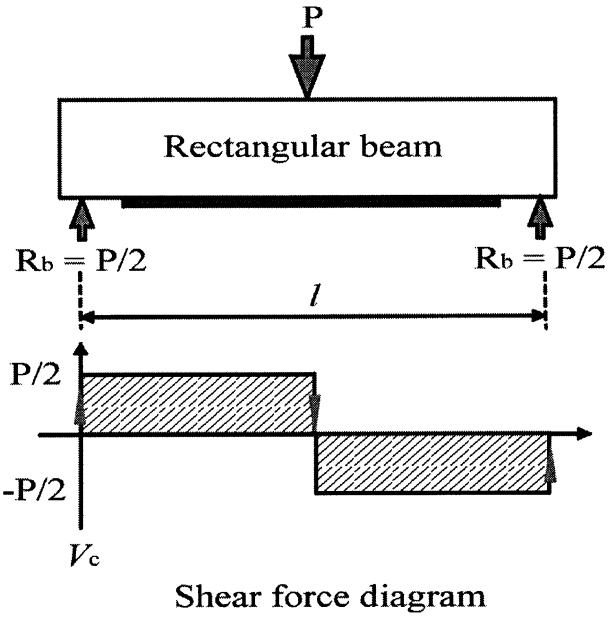

Fig. 6. Shear force diagram of a rectangular beam subjected to a centre-point load.

By considering the force equilibrium condition, the shear force $V_p^z(x)$ at a small element showed in Fig. 5 is determined by

$$\mathrm{d}V_{\mathrm{p}}^{z}(x) = \sigma_{\mathrm{a}}^{z}(x)\omega\,\mathrm{d}x. \tag{32}$$

Then, Eq. (31) can be rewritten as:

$$\frac{\mathrm{d}^2 M_{\mathrm{p}}(x)}{\mathrm{d}x^2} = \sigma_{\mathrm{a}}^{z}(x)\omega - \frac{\mathrm{d}\tau_{\mathrm{a}}(x)}{\mathrm{d}x}\frac{\omega t_{\mathrm{p}}}{2}. \tag{33}$$

The second derivatives of the bending moment of the FRP plate can be expressed as

$$\frac{\mathrm{d}^2 M_{\mathrm{p}}(x)}{\mathrm{d}x^2} = -\frac{\mathrm{d}^4 v_{\mathrm{p}}^{z}(x)}{\mathrm{d}x^4} E_{\mathrm{eff}} I_{\mathrm{p}}, \tag{34a}$$

where

$$E_{\mathrm{eff}} = \frac{1}{\omega t_{\mathrm{p}} A_{11}^{-1}}. \tag{34b}$$

By considering Eq. (29), Eq. (33) can be expressed as

$$\frac{\mathrm{d}^4 v_{\mathrm{p}}^{z}(x)}{\mathrm{d}x^4}\frac{I_{\mathrm{p}}}{t_{\mathrm{p}}\omega\mathbf{A}_{11}^{-1}} + \frac{E_{\mathrm{a}}\omega}{t_{\mathrm{a}}} v_{\mathrm{p}}^{z}(x) = \frac{E_{\mathrm{a}}\omega}{t_{\mathrm{a}}} v_{\mathrm{c}}^{z}(x) + \frac{\mathrm{d}\tau_{\mathrm{a}}(x)}{\mathrm{d}x}\frac{\omega t_{\mathrm{p}}}{2}. \tag{35}$$

By substituting the first derivative of the shear stress function in Eq. (26) into Eq. (35) and we get the following form:

$$\frac{\mathrm{d}^4 v_{\mathrm{p}}^{z}(x)}{\mathrm{d}x^4} + 4\lambda^4 v_{\mathrm{p}}^{z}(x) = 4\lambda^4 v_{\mathrm{c}}^{z}(x) - \frac{C_1\beta(\omega t_{\mathrm{p}})^2 \mathrm{e}^{-\beta x}\mathbf{A}_{11}^{-1}}{2I_{\mathrm{p}}}, \tag{36}$$

where

$$\lambda^4 = \frac{1}{4}\left\{\frac{E_a\omega^2 t_p \mathbf{A}_{11}^{-1}}{I_p t_a}\right\}. \tag{37}$$

Eq. (36) consists of two types of 'load' acting on it: the axial deflections of the concrete $v_c^z(x)$ and the FRP plate $v_p^z(x)$ in the z-direction. For the concrete beam, the axial deflection of the concrete in the z-direction can be evaluated in term of its internal bending moment $M_c(x)$ at any section of x:

$$v_c^z(x) = -\frac{1}{E_c I_c}\int\int M_c(x)\,\mathrm{d}x\,\mathrm{d}x \tag{38}$$

and the bending moment in the concrete is

$$M_c(x) = \int\left(R_b - \tau_a(x)\frac{\omega h}{2}\right)\mathrm{d}x. \tag{39}$$

By substituting Eq. (26) into Eq. (39), we obtain

$$M_c(x) = R_b(x) + \frac{1}{\beta}C_1 e^{-\beta x} - \eta_0 x + D, \tag{40}$$

where D is an arbitrary constant, which can be determined by using an appropriate boundary condition. At the plate end region, $x = 0$, the bending moment in the concrete beam is $M_c(0) = R_b d$. Then, the constant D yields.

$$D = R_b d - \frac{\omega h C_1}{2\beta}. \tag{41}$$

Eq. (38) can then be written as

$$v_c^z(x) = -\frac{1}{E_c I_c}\left\{\frac{1}{6}R_b x^3 + \frac{\omega h}{2\beta^3}C_1 e^{-\beta x} - \frac{\omega h}{12}\eta_0 x^3 + \frac{1}{2}Dx^2 + Fx + G\right\}, \tag{42}$$

where F and G are arbitrary constants. Two boundary conditions are used to solve F and G:

$$v_c^z(-d) = 0 \tag{43a}$$

and

$$v_c^z(0) = -\frac{R_b(3l^2 d - 4d^3)}{24E_c I_c}. \tag{43b}$$

The constants F and G are determined as

$$F = -\frac{1}{d}\left\{\frac{1}{6}R_b d^3 - \frac{\omega h}{2\beta^3}C_1 e^{\beta d} - \frac{\omega h}{12}\eta_0 d^3 - \frac{1}{2}Dd^2 - G\right\} \tag{44a}$$

and

$$G = \frac{R_b(3l^2 d - 4d^3)}{24} + \frac{\omega h}{2\beta^3}C_1. \tag{44b}$$

Let the R.H.S. of Eq. (36) be

$$4\lambda^4 v_c^z(x) - \frac{C_1\beta(\omega t_p)^2 e^{-\beta x}\mathbf{A}_{11}^{-1}}{2I_p} = v_0(x), \tag{45}$$

where

$$v_0(x) = 4\lambda^4\xi_{v1}(x) + 4\lambda^4\xi_{v2}e^{-\beta x} + \xi_{v3}e^{-\beta x} \tag{46}$$

and

$$\xi_{v1}(x) = -\frac{1}{E_c I_c}\left(\frac{1}{6}R_b x^3 - \frac{\omega h}{12}\eta_0 x^3 + \frac{1}{2}Dx^2 + Fx + G\right), \tag{47a}$$

$$\xi_{v2} = -\frac{1}{E_c I_c}\left(\frac{\omega h}{2\beta^3}C_1\right), \tag{47b}$$

$$\xi_{v3} = -\frac{C_1\beta(\omega t_p)^2\mathbf{A}_{11}^{-1}}{2I_p}. \tag{47c}$$

Eq. (36) can then be shortened to

$$\frac{\mathrm{d}^4 v_p^z(x)}{\mathrm{d}x^4} + 4\lambda^4 v_p^z(x) = v_0(x). \tag{48}$$

A differential solution of Eq. (48) is

$$v_p^z(x) = H_1 e^{-\lambda x}\cos(\lambda x) + H_2 e^{-\lambda x}\sin(\lambda x) + v_\lambda(x), \tag{49}$$

where v_λ can be determined by substituting all derivatives of Eq. (49) into Eq. (48):

$$\frac{\mathrm{d}v_p^z(x)}{\mathrm{d}x} = H_1\{-\lambda e^{-\lambda x}(C_{\lambda x} + S_{\lambda x})\} - H_2\{\lambda e^{-\lambda x}(S_{\lambda x} - C_{\lambda x})\} + \frac{\mathrm{d}v_\lambda(x)}{\mathrm{d}x}, \tag{50a}$$

$$\frac{\mathrm{d}^2 v_p^z(x)}{\mathrm{d}x^2} = 2H_1\lambda^2 e^{-\lambda x}S_{\lambda x} - 2H_2\lambda^2 e^{-\lambda x}C_{\lambda x} + \frac{\mathrm{d}^2 v_\lambda(x)}{\mathrm{d}x^2}, \tag{50b}$$

$$\frac{\mathrm{d}^3 v_p^z(x)}{\mathrm{d}x^3} = 2H_1\lambda^3 e^{-\lambda x}(C_{\lambda x} - S_{\lambda x}) + 2H_2\lambda^2 e^{-\lambda x}(C_{\lambda x} + S_{\lambda x}) + \frac{\mathrm{d}^3 v_\lambda(x)}{\mathrm{d}x^3}, \tag{50c}$$

$$\frac{\mathrm{d}^4 v_p^z(x)}{\mathrm{d}x^4} = -4H_1\lambda^4 e^{-\lambda x}C_{\lambda x} - 4H_2\lambda^4 e^{-\lambda x}S_{\lambda x} + \frac{\mathrm{d}^4 v_\lambda(x)}{\mathrm{d}x^4}, \tag{50d}$$

where

$$C_{\lambda x} = \cos(\lambda X) \qquad \text{and} \qquad S_{\lambda X} = \sin(\lambda X). \tag{51}$$

Let $v_\lambda(x)$ be written in the following form:

$$v\lambda(x) = K_1\xi_{v1}(x) + K_2\xi_{v2}e^{-\beta x} + K_3\xi_{v3}e^{-\beta x}. \tag{52}$$

A solution of the fourth derivative of Eq. (52) becomes

$$\frac{\mathrm{d}^4 v_\lambda(x)}{\mathrm{d}x^4} = K_2\beta\xi_{v2}e^{-\beta x} + K_3\beta^4\xi_{v3}e^{-\beta x}. \tag{53}$$

By substituting Eqs. (50a)–(50d) into Eq. (48) and

comparing to Eq. (46):

$$K_2\left(\lambda^4\xi_{v2}\,e^{-\beta x}+\beta^4\xi_{v2}\,e^{-\beta x}\right)+K_3\left(4\lambda^4\xi_{v3}\,e^{-\beta x}+\beta^4\xi_{v3}\,e^{-\beta x}\right)=4\lambda^4\xi_{v2}\,e^{-\beta x}+\xi_{v3}\,e^{-\beta x} \tag{54}$$

and therefore, the coefficients of K_1, K_2 and K_3 are obtained as

$$K_1=1;\qquad K_2=\frac{4\lambda^4}{4\lambda^4+\beta^4}\qquad\text{and}\qquad K_3=\frac{1}{4\lambda^4+\beta^4}. \tag{55}$$

The function of $v_\lambda(x)$ is then determined as follows:

$$v_\lambda(x)=-\frac{1}{E_cI_c}\left(\frac{1}{6}R_bx^3-\frac{\omega h}{12}\eta_0x^3+\frac{1}{2}Dx^2+Fx+G\right)-\frac{4\lambda^4}{4\lambda^4+\beta^4}\frac{1}{E_cI_c}\left(\frac{\omega h}{2\beta^3}C_1\right)e^{-\beta x}-\frac{1}{4\lambda^4+\beta^4}\frac{C_1\beta(\omega t_p)^2\mathbf{A}_{11}^{-1}}{2I_p}e^{-\beta x}. \tag{56}$$

To solve Eq. (49), another two boundary conditions are required. Since the bending moment at the plate end region, $x=0$ is theoretically equal to zero, then

$$\frac{d^2v_p^z(x)}{dx^2}E_pI_p=-M_p(x)|_{x=0}=0 \tag{57}$$

and the shear force $V_{\mathbf{p}}(x)$ is assumed to be zero when $x<0$. The shear stress in the bond line is assumed to reach its maximum value when $x=0$ [17]. The magnitude of this force can then be calculated from Eq. (30), since

$$\frac{d^3v_p^z(x)}{dx^3}=\frac{\omega t_p\mathbf{A}_{11}^{-1}}{I_p}\frac{dM_p(x)}{dx}\bigg|_{x=0}=-\frac{(\omega t_p)^2\mathbf{A}_{11}^{-1}}{2I_p}\tau_{a,max}\bigg|_{x=0}. \tag{58}$$

Consider the first condition:

$$\frac{d^2v_p^z(x)}{dx^2}=-2H_2\lambda^2-\frac{1}{E_cI_c}\left(R_bd-\frac{\omega hC_1}{2\beta}\right)+\frac{\beta^2}{4\lambda^4+\beta^4}\left(\frac{4\lambda^4}{E_cI_c}\left(\frac{\omega h}{2\beta^3}C_1\right)e^{-\beta x}+\frac{C_1\beta(\omega t_p)^2\mathbf{A}_{11}^{-1}}{2I_p}e^{-\beta x}\right)=0. \tag{59}$$

The coefficient H_2 is then calculated:

$$H_2=\frac{1}{2\lambda^2}\left[\frac{\beta^2}{4\lambda^4+\beta^4}\left[\frac{4\lambda^4}{E_cI_c}\left(\frac{\omega h}{2\beta^3}C_1\right)-\frac{C_1\beta(\omega t_p)^2\mathbf{A}_{11}^{-1}}{2I_p}\right]-\frac{1}{E_cI_c}\left(R_bd-\frac{\omega hC_1}{2\beta}\right)\right]. \tag{60}$$

For the second boundary conditions, the third derivative of Eq. (49) with respect to x is

$$2H_1\lambda^3\,e^{-\pi x}(C_{\lambda x}-S_{\lambda x})+2H_2\lambda^3\,e^{-\lambda x}(C_{\lambda x}+S_{\lambda x})-\frac{1}{E_cI_c}\left[R_b+\frac{\omega h}{2}\eta_0\right]+\frac{4\lambda^4\beta^3\,e^{-\beta x}}{4\lambda^4+\beta^4}\frac{\omega h}{2\beta^3E_cI_c}C_1+\frac{\beta^3\,e^{-\beta x}}{4\lambda^4+\beta^4}\frac{\beta(\omega t_p)^2\mathbf{A}_{11}^{-1}}{2I_p}=\frac{(\omega t_p)^2}{2I_p}\tau_{a,max}. \tag{61}$$

The coefficient H_1 is then obtained:

$$H_1=\frac{1}{2\lambda^3}\left\{\frac{(\omega t_p)^2}{2I_p}(C_1+\eta_0)-2H_2\lambda^3-\frac{\xi_{v1}}{E_cI_c}-\frac{\beta^3}{4\lambda^4+\beta^4}(4\lambda^4\xi_{v2}+\xi_{v3})\right\}. \tag{62}$$

So, the peel-off stress of the adhesive material at any section of x can be estimated by following equation:

$$\begin{aligned}\sigma_a^z(x)=\frac{E_a}{t_a}\Bigg\{&\frac{1}{2\lambda^3}\left\{\frac{(\omega t_p)^2}{2I_p}(C_1+\eta_0)-2H_2\lambda^3-\frac{\xi_{v1}}{E_cI_c}-\frac{\beta^3}{4\lambda^4+\beta^4}(4\lambda^4\xi_{v2}+\xi_{v3})\right\}e^{-\lambda x}\cos(\lambda x)\\&-\frac{1}{2\lambda^2}\Bigg(\frac{\beta^2}{4\lambda^4+\beta^4}\left(\frac{4\lambda^4}{E_cI_c}\left(\frac{\omega h}{2\beta^3}C_1\right)-\frac{C_1\beta(\omega t_p)^2\mathbf{A}_{11}^{-1}}{2I_p}\right)\frac{1}{E_cI_c}\left(R_bd-\frac{\omega hC_1}{2\beta}\right)e^{-\lambda x}\\&\times\sin(\lambda x)+\Bigg)+K_1\xi_{v1}(x)+K_2\xi_{v2}\,e^{-\beta x}+K_3\xi_{v3}\,e^{-\beta x}+\frac{1}{E_cI_c}\left\{\frac{1}{6}R_bx^3+\frac{\omega h}{2\beta^3}C_1\,e^{-\beta x}-\frac{\omega h}{12}\eta_0x^3+\frac{1}{2}Dx^2+Fx+G\right\}\Bigg\}.\end{aligned} \tag{63}$$

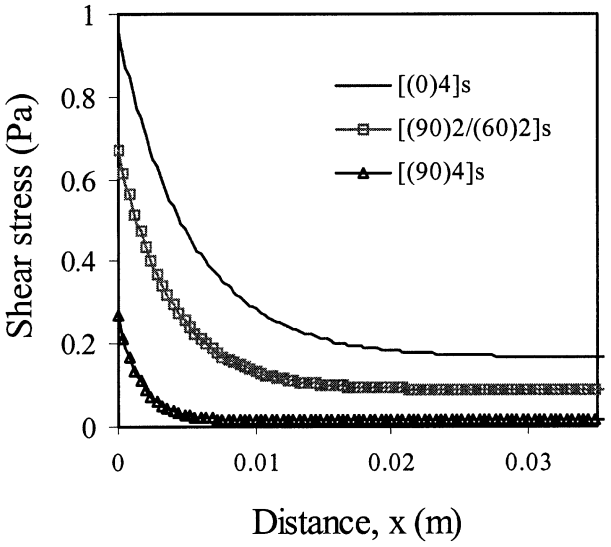

Fig. 7. Adhesive shear stress along the bond line with different fibre orientations ($[(0)_4]_s = 159$ Gpa).

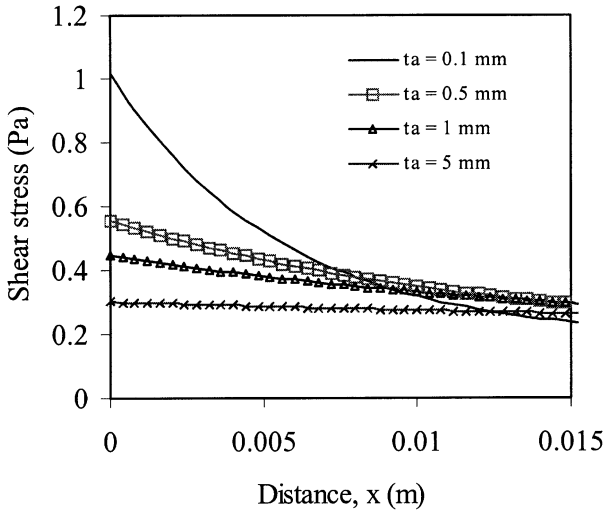

Fig. 9. Adhesive shear stress along the bond line for the FRP strengthened beam with different adhesive thicknesses, t_a.

3. Result interpretations

Eqs. (28a), (28b) and (63) are equations for estimating the adhesive shear and peel-off stresses. The maximum adhesive shear stress is dominated by the coefficient C_1, which is shown in Eq. (23). The tendency of the shear stress distribution and stress transfer length in the adhesive layer for the plate-bonded concrete beam is controlled by a factor of β. Both C_1 and β are functions of the material properties and the geometry of the concrete, the adhesive and the externally bonded composite. Furthermore, the fibre orientation in different laminate layers is also considered in the equation. Any one of these parameters would influence the whole adhesive shear stress distribution along the bond line.

The determination of the adhesive peel-off stress along the bond line is more complicated than the determination of shear stress distribution. Both the beam and FRP plate deformations under bending load conditions are considered as factors that affect the adhesive peel-off stress in the whole system. In fact, the fundamental principle of the adhesive peel-off stress is estimated by Eq. (29). Several parameters such as λ, ξ_{v1}, ξ_{v2}, ξ_{v3}, K_1, K_2 and K_3, would influence the resultant adhesive peel-off stress along the bond line.

Plots of the adhesive shear stress with different fibre orientations, shear modulus and thickness of the adhesive material and the FRP plate are shown in Figs. 7–10. The mechanical properties and geometrical dimensions for the present model are listed in Table 1.

The results shown in the figures clearly indicate that the maximum adhesive shear stress increases with increasing FRP plate tensile and adhesive shear moduli, increasing

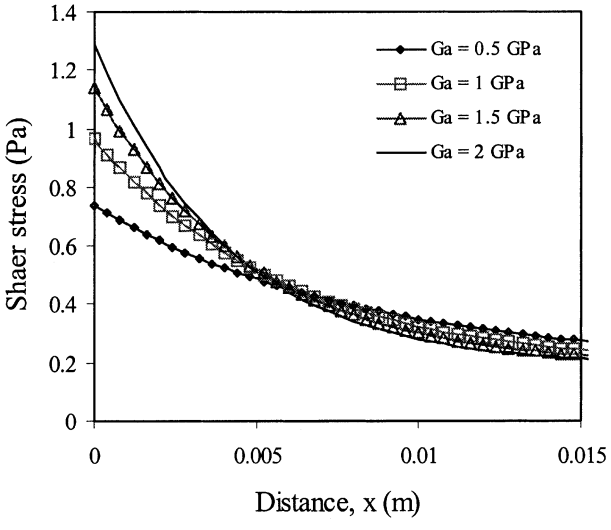

Fig. 8. Adhesive shear stress along the bond line for the FRP-strengthened beam with different adhesive shear modulus, G_a.

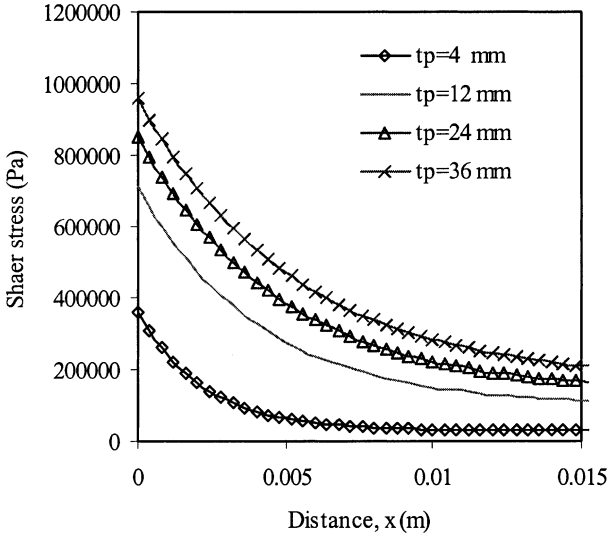

Fig. 10. Adhesive shear stress along the bond line for the FRP-strengthened beam with different plate thickness, t_p.

Table 1
Dimensions and material data used in the present example

E_a (GPa)	G_a (GPa)	t_a (mm)	E_p $[(0)_4]_s$ (Gpa)	E_c (GPa)	H (GPa)	ω (mm)	t_p (mm)	d (mm)	L (mm)	P (kN)
3.3	1.15	0.1–5	159	27.8	0.15	0.15	0.8–8	0.025	0.35	17

thickness of the FRP plate, and decreasing thickness of the adhesive layer. The maximum adhesive shear stress also increases with increasing alignment of all high strength fibres in the composite plate in beam's longitudinal direction x. Figs. 7–10 show that the maximum adhesive shear stress is at the plate end region $x = 0$ and rapidly vanishes with increasing length toward the centre of the beam. Fig. 11 compares the maximum adhesive shear stress with different numbers of laminate layers, adhesive shears and plate moduli. The adhesive peel-off stress with the different fibre orientations, shear moduli, thicknesses of the adhesive material and numbers of laminate layers are plotted in Figs. 12–15.

According to the predicted results, the adhesive peel-off stress increases with increasing FRP plate tensile and adhesive shear moduli, increasing numbers of laminate layers, and decreasing thicknesses of the adhesive layer. The maximum adhesive peel-off stress is reached at the plate end region and then rapidly decreases to a negative value in general. Near-zero stress is obtained when moving further toward the centre of the beam. The stress-affected zone is highly dependent on the material properties and geometrical factors. The formation of a negative peel-off stress region is due to the upward bending of the externally bonded FRP plate with high adhesive shear stress at the plate end region.

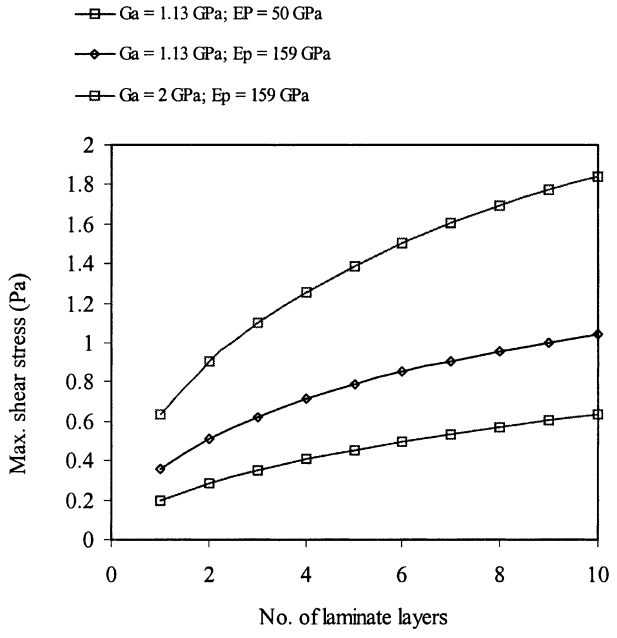

Fig. 11. Comparison of the maximum adhesive shear stress with different numbers of laminate layers, adhesive shear and plate moduli.

In general, high modulus plates have been used for concrete rehabilitation and repair. However, the induced adhesive shear and peel-off stresses cannot be ignored. These stresses may cause premature failure at a load that is below the estimated maximum strength of the FRP-strengthened structure.

The use of an FRP plate with different fibre orientations results changes the effective modulus E_{eff} of the composite plate. Having high strength fibres aligned in the beam direction would maximise the modulus of the plate, while having the fibres aligned perpendicularly to the beam axis would greatly reduce the plate modulus. The effects on adhesive shear stress with different fibre orientation measured from the beam's longitudinal direction are shown in Fig. 16.

4. Result validation

Since the adhesive shear stress cannot be measured directly through experimentally, finite element method (FEM) was used to validate the results from the theoretical prediction. The Msc/Nastran 4.0 commercial FEM package was used to model and analyse the rectangular beam strengthened by an externally bonded FRP plate subjected to the three-point bending load. The tensile modulus of the concrete and FRP plate, and the shear moduli of the adhesive material of 27.8, 159 and 1.125 GPa were

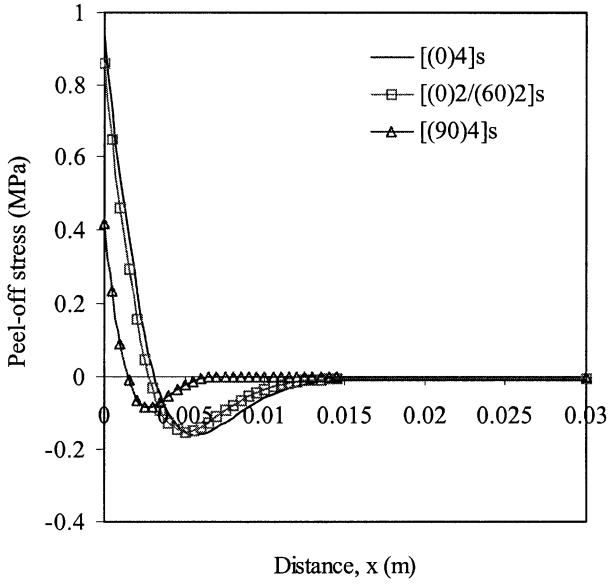

Fig. 12. Adhesive peel-off stress along the bond line with different fibre orientations ($[(0)_4]_s = 159$ Gpa).

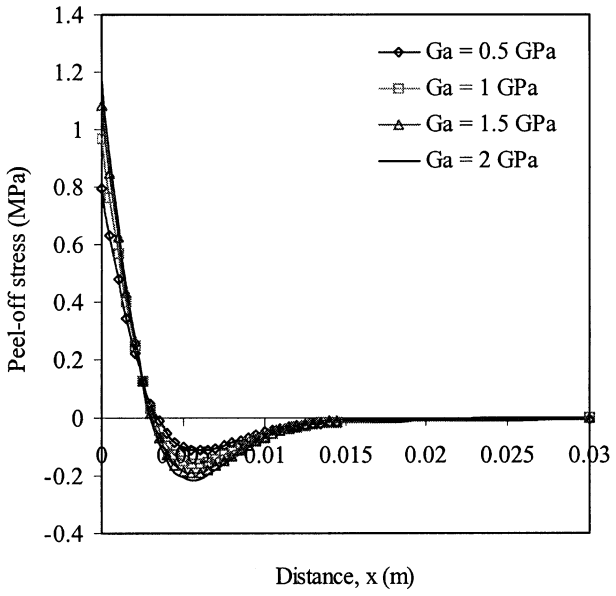

Fig. 13. Adhesive peel-off stress along the bond line for the FRP-strengthened beam with different adhesive shear moduli, G_a.

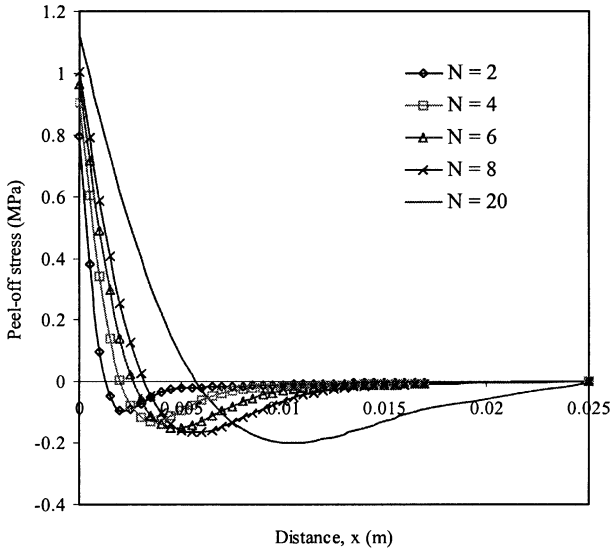

Fig. 15. Adhesive stress along the bond line for the FRP-strengthened beam with different numbers of laminate layers, N.

modelled to study the stress transferring properties in the adhesive material with a centre applied load of 17 kN. The thicknesses of the adhesive layer and plate are 0.1 and 1.6 mm, respectively. Since the beam is symmetrical about its centre axis, only half of the beam with appropriate constraints at the centreline was modelled.

In the present study, different mesh sizes in the adhesive layer were used to test the convergence and the resultant adhesive shear stresses at the plate end are listed in Table 2. To minimise the processing time while maintaining the accuracy of the results, plate elements (Quad 4) with a mesh size of 156.25 μm were selected at the plate end region. The FEM model for validating the theoretical result is shown in Fig. 17. The FEM model has been validated with the experimental results from a concrete beam strengthened by three layers of glass fibre composite on its tension surface. The results of the tensile strain extracted from the experiment and FEM solution are plotted in Fig. 18.

The results from the FEM analysis together with the theoretical prediction for interfacial shear and peel-off stresses of the FRP plate are shown in Figs. 19 and 20, respectively, It can be concluded that only a very fine mesh can show the descending branch in the shear stress very close to the plate end region. The result from the

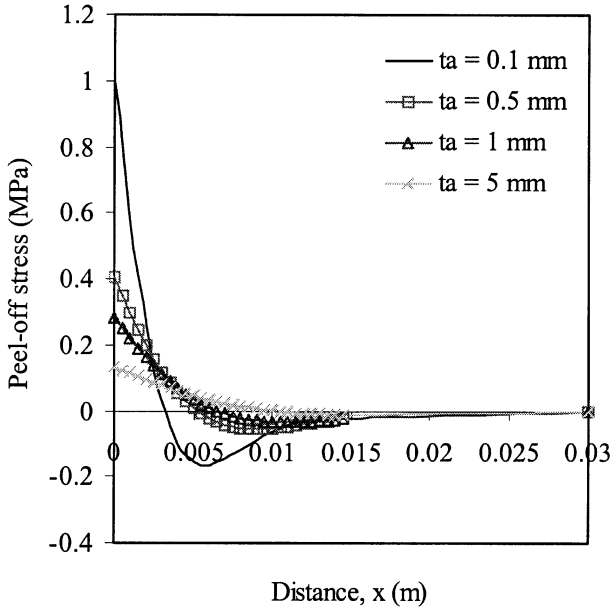

Fig. 14. Adhesive peel-off stress along the bond line for the FRP-strengthened beam with different adhesive thicknesses; t_a.

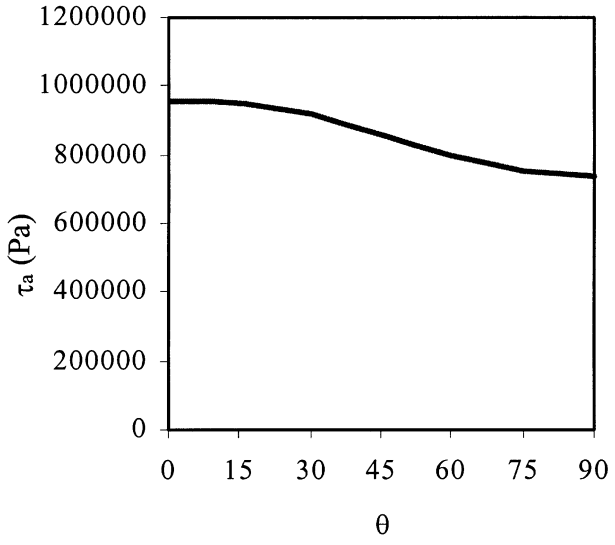

Fig. 16. Effects on adhesive shear stress with different fibre orientation (through the whole laminate layers) measured from the beam's longitudinal axis.

Table 2
Results from the convergence test for different mesh sizes FEM model

Mesh size (mm)	0.625	0.3125	0.15625	0.78125	0.03915
$\tau_{a,\,max}$ (MPa)	0.752	0.821	0.957	0.971	0.978

adhesive shear stress shows a slight deviation from the FEM solution at the plate end region. However, at the location of maximum stress, which is used for design, the agreement between the FEM result and present method is good, as can be seen from Figs. 19 and 20. In general, both the adhesive shear and peel-off stresses estimated from the theoretical study compare well with the FEM solutions. In this study, it is possible to calculate the critical stress levels for the adhesive material at the end of the outer FRP plate by using linear elastic theory.

Indeed, the mechanical properties of the FRP materials behave in orthotropic forms. However, Malek et al. [18] pointed out that the variation of the elastic modulus in the transverse direction does not have a significant effect on shear and peel-off stresses of the composite-strengthened beam system. Therefore, the present theoretical prediction is valid for estimating the critical stress in the adhesive materials.

5. Cracked concrete beam

For a cracked concrete beam, the axial load of the FRP plate at the crack-mouth region cannot be evaluated by using Eq. (27) since the stress distribution along the mid-beam axis, y is no longer in linear elastic form. Therefore, the linear elastic theory cannot be used to determine the axial stress of the FRP plate in the mid-beam region. However, Lau et al. [19] proposed a simple superposition method to evaluate the plate normal stress for the cracked beam with an externally bonded FRP reinforcement on the beam tension surface, i.e.

$$N_{\mathrm{p}} = \frac{\omega\sqrt{\pi a_{\mathrm{e}}}}{2f_{\mathrm{F}}(\alpha)}\{K_{\mathrm{M}} - K_{\mathrm{IA}}\}. \tag{64}$$

Therefore, the adhesive shear and peel-off stresses for the FRP-bonded concrete structure can then be evaluated by

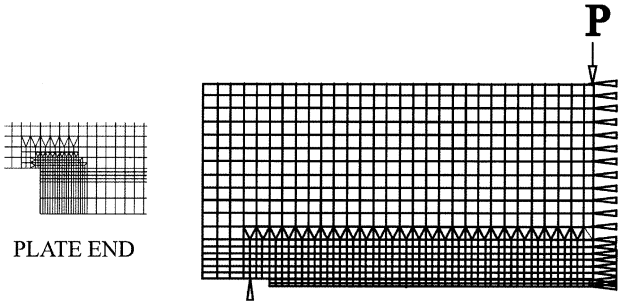

Fig. 17. The FEM model for validating the results from the theoretical prediction.

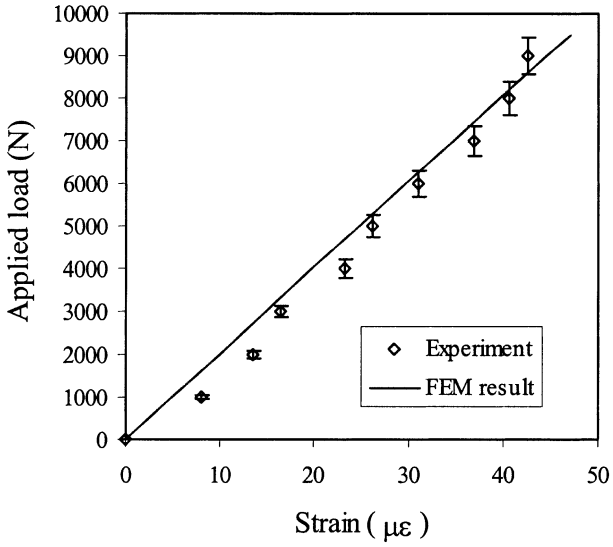

Fig. 18. Comparison of the FEM model and the experiment.

using the boundary condition at the crack section ($x = L/2$) for Eq. (27). The coefficient of C_1 is then determined:

$$C_1 = \frac{N_{\mathrm{p}}\beta}{\omega} - \frac{L}{2d}. \tag{65}$$

Therefore, by knowing the axial load in the externally bonded FRP plate, the maximum adhesive shear stress at the plate end regions can be evaluated. In fact, for a concrete beam with crack initiation, debonding at the interface of the FRP plate at the crack opening and reinforcing steel pull-out action usually happens due to the action of crack movement. Therefore, to apply the current model to reinforced concrete (RC) structures, a closing force, which reduces the bending moment of the beam due to the steel bar pull-out friction, should be considered in Eq. (11).

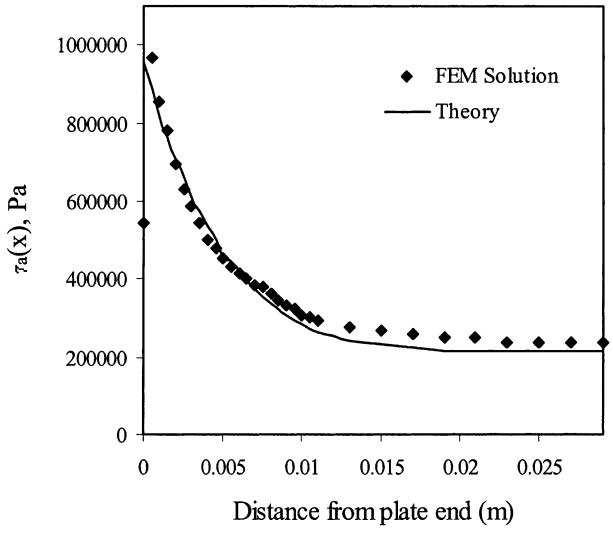

Fig. 19. Comparison of the adhesive shear stresses obtained from the FEM and the theoretical prediction.

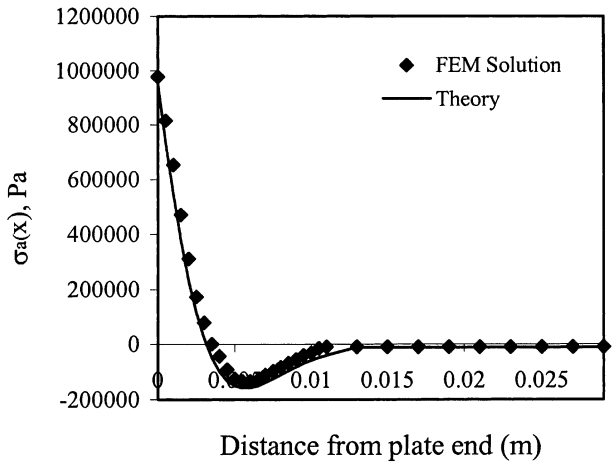

Fig. 20. Comparison of the adhesive peel-off stresses obtained from the FEM and the theoretical prediction.

6. Conclusions

In the present study, only a plain rectangular concrete beam without internal reinforcement is considered. Throughout this study, we can conclude that the proposed theoretical model is able to determine the shear and peel-off stresses of the adhesive layer, and the axial force in the FRP plate for the FRP-strengthened concrete element. The theoretical predictions compare well with the experimentally validated FEM solutions. Different fibre arrangements inside the FRP laminate are considered in evaluating the stress mechanism of the strengthened structures. The effective modulus of the externally bonded FRP plate increases with increasing percentage of fibre aligned in the beam's longitudinal direction. The maximum shear and peel-off stresses increase with increasing moduli of the FRP plate and adhesive materials and decreasing thickness of the adhesive layer.

The design of the FRP-strengthened concrete system should consider the resultant adhesive shear and peel-off stresses, the axial stress in the FRP plate and the allowable shear stress and stress intensity factor of the beam due to the external applied load, and it should optimise the fibre orientation and laminate arrangement in order to achieve the maximum strengthening capability.

Recently, it was found that plate peeling at the plate/glue/concrete interface is, indeed, very rare due to strong chemical bonding of adhesive materials to the concrete. This is usually attributed to bad workmanship. However, a high peel-off stress may cause the plate and concrete to separate as a unit from the underside of the steel reinforcement.

In future, more extensive work is required to solve the problems caused by fire, vandalism and fatigue damages of the concrete and bonding interface of FRP-strengthened concrete structures.

Acknowledgements

This research project was funded by The Hong Kong Polytechnic Research Grant G-V528 and the Research Grant Council of Hong Kong (PolyU 5160/99E).

References

[1] Seible F, Priestley MJN, Hegemier GA, Innamorato D. Seismic retrofit of RC columns with continuous carbon fibre jackets. J Comp Constr 1997;1(2):52–62.
[2] Mo YL, Tsai SP, Lee IS. Seismic performance behaviour of beam-column connections in pre-stressed concrete bridges. J Mater Struct 1998;31:411–7.
[3] Hamoush A, Ahmad SH. Concrete crack repair by stitches. J Mater Struct 1997;30(201):418–23.
[4] Connor JSO. New York State gives FRP's a try. Structure Magazine, Summer 1999.
[5] Lau KT, Zhou LM, Woo CH. Strengthening and strain monitoring concrete structures using fibreglass composites and FBG sensor. J Mater Sci Res Int 1999;5(3):216–21.
[6] Varastehpour H, Hamelin P. Strengthening of concrete beams using fibre-reinforced plastic. J Mater Struct 1997;30:160–6.
[7] Malek AM, Saadatmanesh H, Ehsani MR. Prediction of failure load of RC beams strengthened with FRP plate due to stress concentration at the plate end. ACI Struct J 1998;95(1):142–52.
[8] Dutta PK. Fatigue testing of composite bridge decks under extreme temperatures. ProcSeventh Int Conf Compos Engng 2000:755–6.
[9] Lau KT, Zhou LM. Mechanical performance of composite-strengthened concrete structures. J Comp Part B 2001;32(1):21–31.
[10] Tripi JM, Bakis CE, Boothby TE, Nanni A. Deformation in concrete with external CFRP sheet reinforcement. J Compos Constr 2000;4(2):85–94.
[11] Lau KT, Zhou LM, Ye L, Diao M. Investigation on upgrading and health monitoring the civil concrete structures using FRP and FBG sensor. Adv Compos Lett 1999;8(6):323–32.
[12] Ramana VPV, Kant T, Morton SE, Dutta PK, Mukherjee A, Desai YM. Behaviour of CFRC strengthened reinforced concrete beams with varying degrees of strengthening. J Comp Part B 2000;31:461–70.
[13] Hyer MW. Stress analysis of fibre-reinforced composite material. USA: McGraw Hill, 1998.
[14] RMIT. Design and manufacture of advanced fibre composite structures — a practical course in the application of advanced composite technology. Published by Royal Melbourne Institute of Technology University, 1996.
[15] Lau KT, Zhou LM, Wu JS. Investigation on strengthening and strain sensing technique for concrete structure. J Mater Struct 2001;34:42–50.
[16] Triantafillou TC, Deskovic N, Deuring M. Strengthening of concrete structures with pre-stressed fibre reinforced plastic sheets. ACI Struct J 1992;89(3):235–44.
[17] Taljsten B. Strengthening of beam by plate bonding. J Mater Civil Engng 1997;9(4):205–12.
[18] Malek AM, Saadatmanesh H, Ehsani MR. Prediction of failure load of RC beams strengthened with FRP plate due to stress concentration at the plate end. ACI Struct J 1998;95(1):142–52.
[19] Lau KT, Shi SQ, Zhou LM. Estimation of stress intensity factor (K_I) for the plate bonded concrete beams by using superposition method. Mag Concr Res 2001;53:31–41.